ACS OMEGA

Open Access

http://pubs.acs.org/journal/acsodf

Article

Selective Sensing of DNA Nucleobases with Angular Discrimination

Published as part of ACS Omega virtual special issue "Nucleic Acids: A 70th Anniversary Celebration of DNA".

Laith A. Algharagholy, Víctor Manuel García-Suárez,* and Sawsan S. Abaas

Cite This: *ACS Omega* 2024, 9, 3240−3249

Read Online

ACCESS | Metrics & More | Article Recommendations | Supporting Information

ABSTRACT: The fast and precise selective sensing of DNA nucleobases is a long-pursued method that can lead to huge advances in the field of genomics and have an impact on aspects such as the prevention of diseases, health enhancement, and, in general, all types of medical treatments. We present here a new type of nanoscale sensor based on carbon nanotubes with a specific geometry that can discriminate the type of nucleobase and also its angle of orientation. The proper differentiation of nucleobases is essential to clearly sequence DNA chains, while angular discrimination is key to improving the sensing selectivity. We perform first-principle and quantum transport simulations to calculate the transmission, conductance, and current of the nanotube-based nanoscale sensor in the presence of the four nucleotides (A, C, G, and T), each of them rotated 0, 90, 180, or 270°. Our results show that this system is able to effectively discriminate between the four nucleotides and their angle of orientation. We explain these findings in terms of the interaction between the phosphate group of the nucleotide and the nanotube wall. The phosphate specifically distorts the electronic structure of the nanotube depending on the distance and the orientation and leads to nontrivial changes in the transmission. This work provides a method for finer and more precise sequential DNA chains.

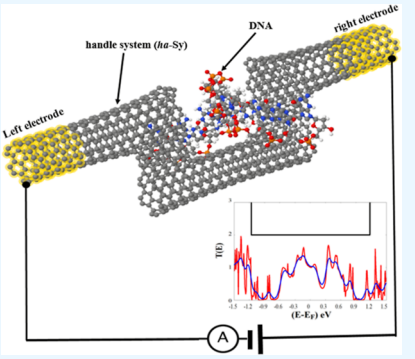

INTRODUCTION

Deoxyribonucleic acid (DNA) sequencing, which is a widely known process to provide essential information for functioning of living systems,[1,2] human genomic imprint,[1−3,3] disease diagnosis,[2,4,5] and biomedical treatments,[6,7] plays a significant role in human health improvement.[8] DNA is a one-dimensional polymer[9−12] composed of four nucleic acid bases, namely, adenine (A), cytosine (C), guanine (G), and thymine (T). Each of the nucleobases is attached to a backbone made of sugar (deoxyribose) and phosphate, making a nucleotide. The sequence of DNA nucleobases can then be considered as a memory that stores genetic information ingrained in individual organisms.[12] Since the original idea of using DNA to construct structures,[13−15] which was first proposed by Ned Seeman 40 years ago (early 1980s), the field of DNA sequencing[9,16−29] has received enormous interest among scientists and researchers. In order to successfully sequence DNA, the development of nanoscale sensors plays a fundamental role. Previous publications have reported that low-dimensional nanomaterials, including heteronanomaterials, can be promising candidates for selective sensing applications, including the detection of explosives,[30−35] the selective sensing of gases,[36−39] the detection of environmental pollutants,[40−42] and the development of biosensors.[43−48] Regarding DNA sequencing, a number of techniques have been established in the past few years, such as optical selective sensing methods using fluorescent labeling of biomolecules and Sanger sequencing detection approaches (chain termination) for regions of DNA of approximately 900 nucleobase pairs in length. However, such methods are rather expensive and time-consuming.[9,49−52] On the other hand, a variety of alternative and promising strategies based on nanoscale elements have been developed, such as the use of single molecules, which show the possibility of accurately interrogating the nucleobase sequence,[12,53−56] or the use of solid-state nanogaps/nanopores.[9,25,57−59] However, faster, less expensive, and label-free approaches for discriminating small molecules such as the DNA nucleotides are still needed and can be considered highly desired targets of current technology.[12,30,60]

In order to overcome current challenges in designing selective sensing nanodevices for DNA sequencing and to be able to fabricate effective, portable, efficient, and cheap selective sensing nanodevices, it is necessary to develop novel nanostructured materials and concepts and devise new scenarios for managing and developing nanosensor chips. Since it is not necessary to separate transduction from the application of an electrical signal using well-fitted electrical strategies for DNA sequencing, it should be possible to accomplish selective sensing at low cost (compared to

Received: July 11, 2023
Accepted: September 25, 2023
Published: January 10, 2024

conventional methods[9,22,61]) electrochemical analyzers. On the other hand, previous studies[9,62,63] have also reported that DNA, which shows outstanding electrical characteristics, including conducting, semiconducting, and insulating properties, can interact with single-walled carbon nanotubes (SWCNTs) under various configurations[64−66] and can also significantly affect their electrical conductance.[30,52,67,68] The nanotubes are, in general, highly sensitive to their surrounding environment, and their electronic properties can be significantly altered by the adsorption of various chemicals and biomolecules on their surface. This fact makes SWCNTs very promising nanomaterials for label-free and selective sensing applications. In fact, these systems have already been used as nanogaps for sensing DNA.[69,70] Herein, we propose a proof of work system where we have designed and studied a specific geometry of carbon nanotubes (CNT), a handle-like system that we refer to as *ha*-Sy, shown in Figure 1 with a strand of DNA passing through it, which is especially suited for selective sensing of DNA. Besides, the proposed system tries to solve problems that might arise in other DNA sequencers, such as nanopores, where, if the size of the pore is not adequate, the DNA might get stuck (pore too small) or pass leaving a small signal (pore too big). The open side of this design should give the DNA strand more freedom to pass through it and allow for smoother sequencing. Note as well that the $\pi-\pi$ interaction of the DNA strand with the nanotube walls should favor its insertion into the handle system and keep it inside since in that place the interaction with the walls is larger (this is also confirmed by the binding energy, as we shall see).

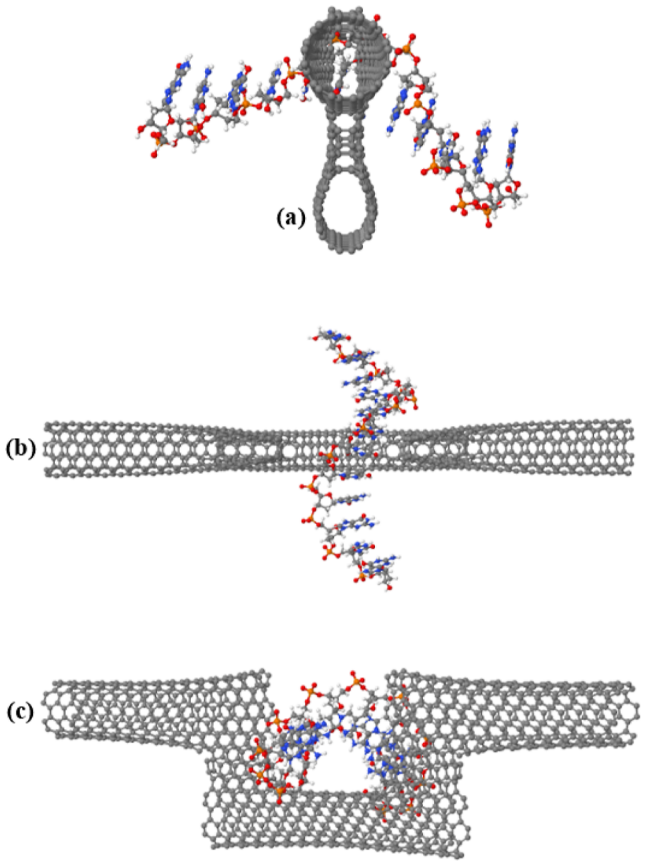

Figure 1. Side (a), top (b), and front (c) view of a DNA strand passing through the handle system (*ha*-Sy).

RESULTS AND DISCUSSION

To obtain the *ha*-Sy, we used the sculpturene method,[71] a methodology that allows to build unique forms of sp^2-bonded molecular structures, such as deterministic CNT from a spontaneous reconstruction of bilayer graphene nanoribbons or heterobilayer nanoribbons. The principle of this methodology consists of sculpting (cutting) selected/desired shapes of nanoribbons out of bilayer graphene in vacuo, something that can be accomplished experimentally with, for example, scanning tunneling microscope lithography,[72] and allowing the shapes to reconstruct globally to finally make unique molecular structures. This procedure opens new avenues for the creation of novel nanomaterials with unique geometries. For instance, the formation of T-shaped and cross-shaped compositions of nanotubes with the same or different chiralities.[71,73] We initially prepared the *ha*-Sy by starting with AA-stacked bilayer graphene (biG) and then sculpted the biG into zigzag graphene nanoribbons with a handle-like shape, as shown in Figure 2a,b. The resulting reconstruction leads to the formation of the *ha*-Sy shown in Figure 2c,d, which consists of (6,6) CNT as left/right leads connected in a 90° turno to (5,5) CNT in the scattering region. Experimentally, the folded edges can be formed by cutting bilayer/multilayer graphene, as has been shown in various experiments.[74−76] The stability of the closed structure relative to that with open edges can also be proven by calculating the total energy of both cases. In the closed edges case, the energy (−1,72,181.88 eV) is much smaller than in the open edges case (−1,71,626.73 eV), which is also expected by the presence of unsaturated dangling bonds in the later. Such stability can also be further compared with that of CNT by calculating the average binding energy per atom (total energy of the system divided by the number of atoms minus the energy of an isolated carbon atom), and surprisingly, the handle turns out to be more stable than the (5,5) and (6,6) CNTs since it has a smaller average binding energy (−10.75 eV vs 8.87 and −8.92 eV for the (5,5) and (6,6) CNTs, respectively). Notice as well that topologically, sculpturene molecular structures made of nanotubes are stable against atomic-scale defects.[71]

In this work, we aim to examine the capability of *ha*-Sy for DNA sequencing. Before that, and, to understand the conductance of the bare *ha*-Sy (Figure 2c) as a reference system to compare with that in contact with the nucleotides, we investigate its transmission $T(E)$. As can be seen, the resulting $T(E)$ shows no energy gap (E_g) and has sizable values around the Fermi level, as shown in Figure 3. This indicates that the system retains metallic-like properties, even though it has a nontrivial geometry constructed with different nanotubes.

After obtaining the *ha*-Sy, we place the four DNA nucleobases (A, C, G, and T) inside the *ha*-Sy with various orientation angles (0, 90, 180, and 270°) as shown in Figures 3 and S1−S3. As commented before, each nucleobase is also attached to a phosphate and a deoxyribose, forming a nucleotide, which is the part of the DNA that enters the sensor. Notice that, due to computational limitations, the use of individual nucleotides is obviously a simplification with respect to the inclusion of a real DNA chain, where the phosphates of different nucleotides are joined together, making the DNA backbone. However, these configurations still retain the main interactions between the nucleotides and the sensor (which essentially depend on the distance between the phosphate group and the nanotube, as we shall see) and

https://doi.org/10.1021/acsomega.3c04945
ACS Omega 2024, 9, 3240−3249

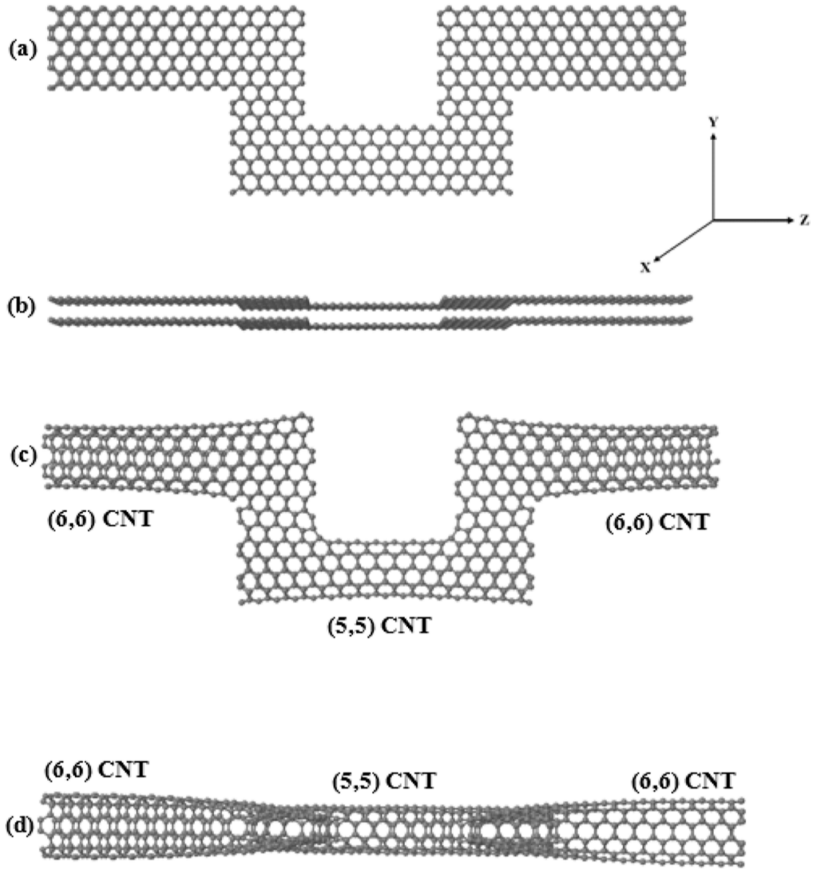

Figure 2. (a) AA-stacked zigzag bilayer graphene (side view) which contains 1110 carbon atoms, (b) top view of the initial supercell in (a), and (c) side view and (d) top view of the obtained *ha*-Sy. The initial supercell is periodic in the *Z* direction and finite in the *X* and *Y* directions.

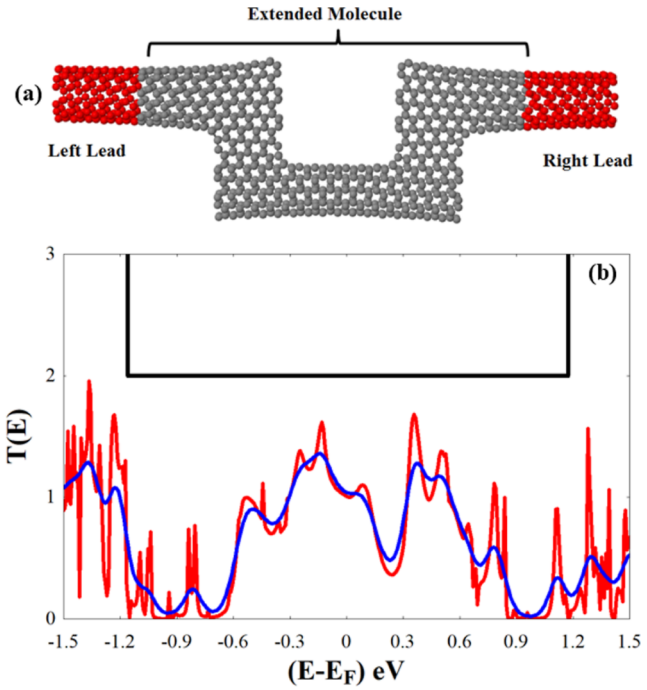

Figure 3. (a) Handle system (*ha*-Sy); the red-shaded region represents the (6,6) CNTs as left/right leads, while the gray-shaded region represents the scattering region, which includes the (5,5) CNT. (b) Transmission $T(E)$ of the bare *ha*-Sy (red line) and the room-temperature electrical conductance G (blue line).

should give a response very similar to that of a nucleotide in a full DNA chain. Later on, we relax the *ha*-Sy with the nucleotides, each of them with the four possible angles. Figure 4 shows, for instance, the *ha*-Sy with an A nucleotide (*ha*-Sy + A) in the four orientation angles.

To find the relaxed geometry and ground-state Hamiltonian of all systems (bare *ha*-Sy and *ha*-Sy with nucleotides) shown in Figures 1, 3, and S1−S3, we used the SIESTA[77] implementation of density functional theory, with the local density approximation[78] parameterized with the Ceperley−Alder exchange correlation functional and a double-ζ polarized basis sets of pseudoatomic orbitals. The initial supercell was optimized until all the forces were smaller than 0.005 eV/Å. The system was made periodic along the *Z* direction, while, to ensure that there was no interaction between neighboring cells along the perpendicular directions, vacuum spaces of 60 and 100 Å were added along the *X* and *Y* directions, respectively. For the left/right leads calculations, a *k*-point grid of 1 × 1 × 25 in the Brillouin zone was employed. Once the final handle-like system (*ha*-Sy) was built, the mean-field Hamiltonian and overlap matrices produced by SIESTA were exported to the quantum transport code GOLLUM[79] and used to calculate the low bias transmission probability $T(E)$ for electrons of energy (E) passing from the left lead (source) to the right lead (drain) through the scatterer and the *IV* (current−voltage) characteristics.

We investigate first the electronic properties of the bare *ha*-Sy system (scattering region) by calculating the density of states (DOS), shown in Figure S4, which has a finite value at the Fermi level and shows that the system is metallic. When

https://doi.org/10.1021/acsomega.3c04945
ACS Omega 2024, 9, 3240−3249

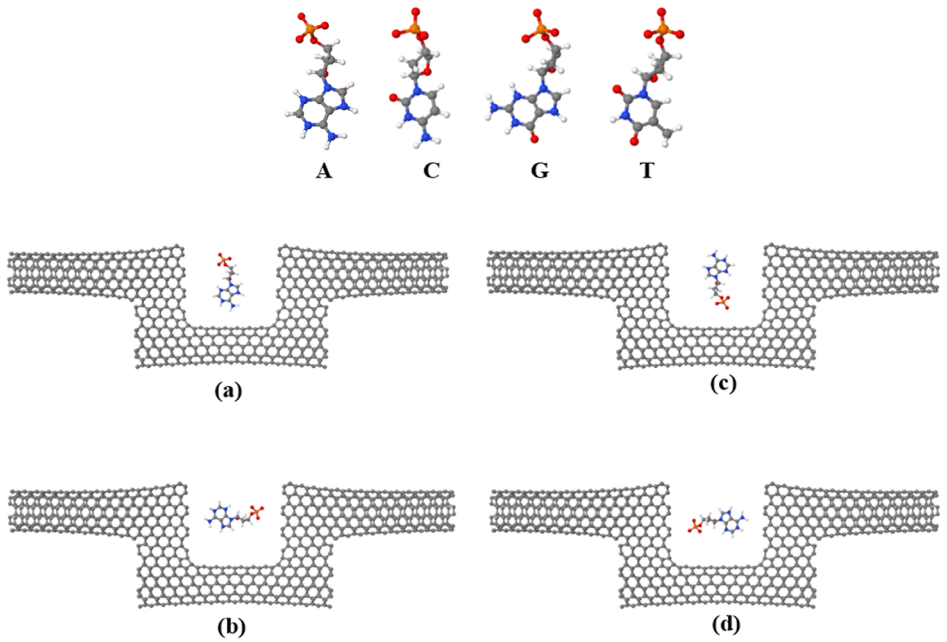

Figure 4. Top subfigure shows the molecular structure of the four nucleobases of DNA: adenine (A), cytosine (C), guanine (G), and thymine (T). Each nucleobase is attached to a phosphate and a deoxyribose. (a−d) Relaxed *ha*-Sy with an A nucleotide in four different orientations: 0, 90, 180, and 270°, respectively.

Table 1. Charge Transfer between Each Molecule and the *ha*-Sy[a]

ha-Sy	CT	*ha*-Sy	CT	*ha*-Sy	CT	*ha*-Sy	CT
+A with 0°	0.008*e*	+C with 0°	0.005*e*	+G with 0°	−0.010*e*	+T with 0°	−0.001*e*
+A with 90°	0.010*e*	+C with 90°	0.005*e*	+G with 90°	−0.013*e*	+T with 90°	−0.005*e*
+A with 180°	0.009*e*	+C with 180°	0.004*e*	+G with 180°	−0.008*e*	+T with 180°	−0.006*e*
+A with 270°	0.007*e*	+C with 270°	0.006*e*	+G with 270°	−0.009*e*	+T with 270°	−0.003*e*

[a]A positive sign means that the charge is transferred from *ha*-Sy to the molecule, while a negative sign means that the charge is transferred from the molecule to the *ha*-Sy.

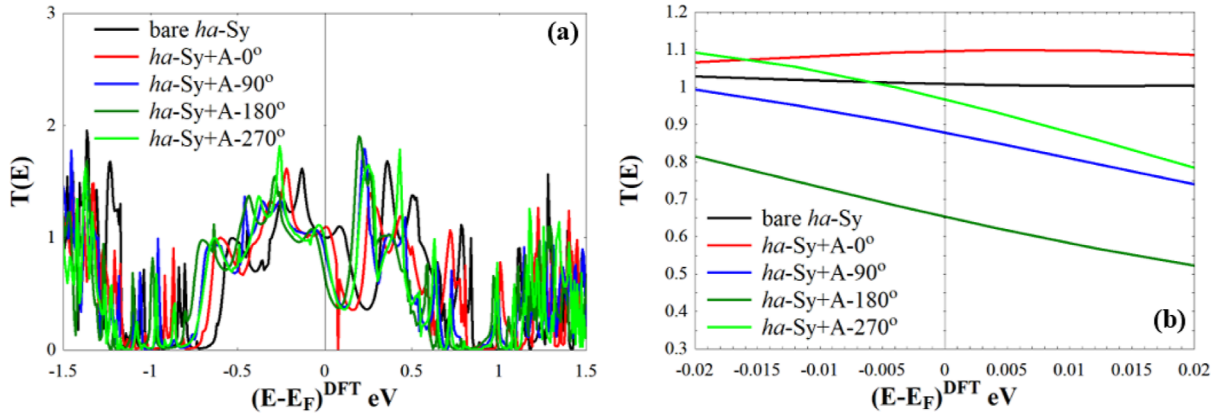

Figure 5. (a) $T(E)$ of the *ha*-Sy + A with four different angles of orientation (0, 90, 180, and 270°), and (b) $T(E)$ in a narrow energy window (−0.02 to 0.02 eV) around E_F.

the nucleotides are included, we also performed additional calculations to get further details about the electronic structure, such as the charge transfer, which is in general rather small (see Table 1). The sign is positive in general (transferred from the *ha*-Sy to the molecule) for A and C and negative (transferred from the molecule to *ha*-Sy) for G and T. Such small values are expected since both systems are stable and weakly coupled. We also checked the stability of the system by calculating the binding energy, defined as $E_B = E^{haSy+Nuc} - (E^{haSy}_{G,Nuc} + E^{Nuc}_{G,haSy})$, where $E^{haSy+Nuc}$ represents the total energy of the whole system, i.e., the *ha*-Sy and the nucleotide, $E^{haSy}_{G,Nuc}$ is the energy of the *ha*-Sy in the presence of the ghost states of the nucleotide, and $E^{Nuc}_{G,haSy}$ is the energy of the nucleotide in the presence of the ghost states of the *ha*-Sy. The binding energies are negative and in an absolute value smaller than 0.6 eV, which means that the nucleotides will not be repelled by the *ha*-Sy and will tend to pass through it.

https://doi.org/10.1021/acsomega.3c04945
ACS Omega 2024, 9, 3240−3249

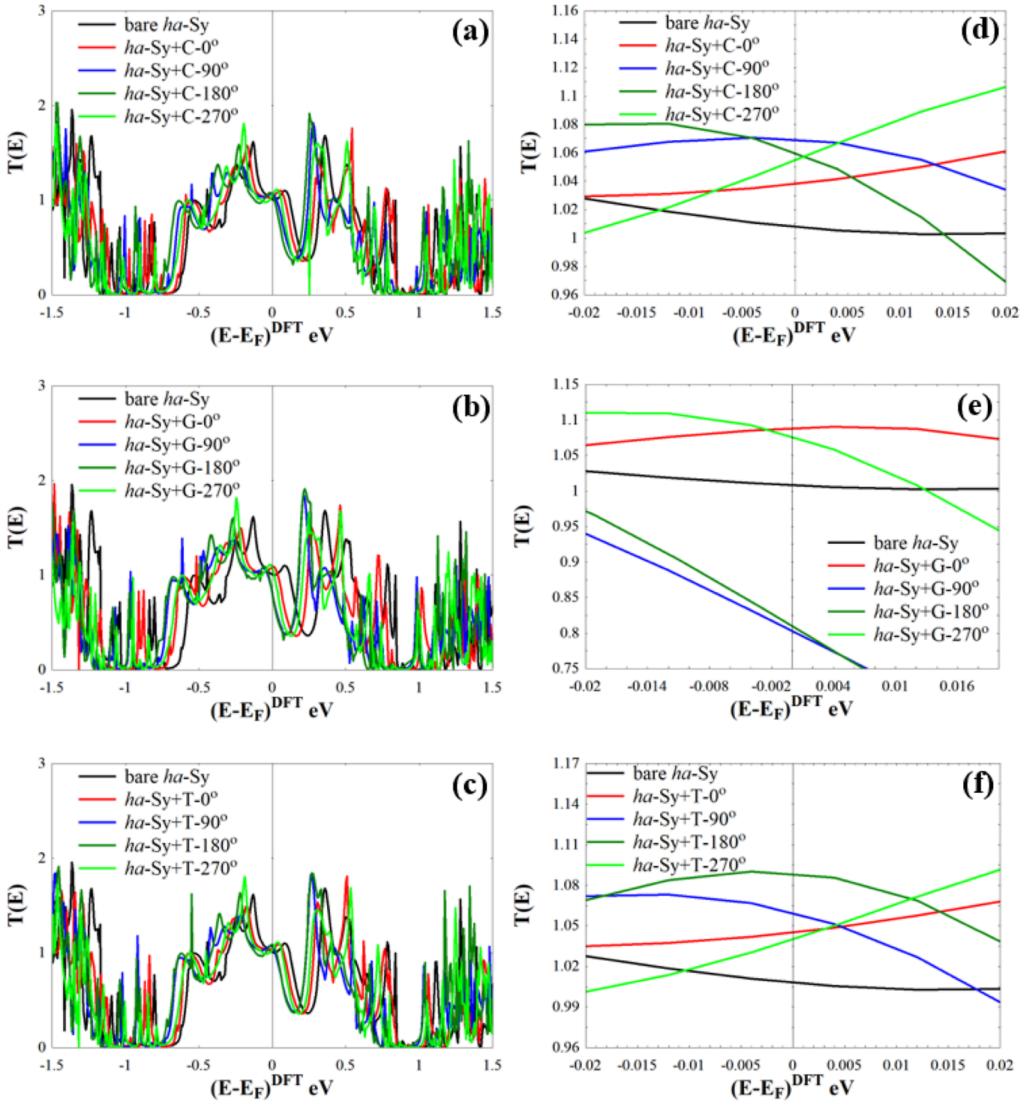

Figure 6. (a–c) $T(E)$ of *ha*-Sy with C, G, and T nucleotides (*ha*-Sy + C, *ha*-Sy + G, and *ha*-Sy + T) shown in Figures S1–S3, respectively. All nucleotides are oriented with four possible angles (0, 90, 180, and 270°). (d–f) $T(E)$ in a narrow energy window (−0.02 to 0.02 eV) around E_F.

In what follows, we use computed $T(E)$ and IV to investigate the ability of the *h*a-Sy to discriminate the four DNA nucleobases. Figure 5 shows the transmission of *h*a-Sy + A. From this figure, it is clear that $T(E)$ depends on the orientation of the A nucleotide inside the *ha*-Sy. This means that rotating the A nucleotide inside *ha*-Sy leads to noticeable changes in $T(E)$. We can also see that *ha*-Sy + A with 0° increases $T(E)$, whereas the cases with 90, 180, and 270° decrease it. The asymmetric geometry along the Y direction of the *ha*-Sy sensor provides an effective shape for discriminating between the orientation of the nucleotides, as compared to previous nanoscale sensors based on nanogaps/nanopores,[9,25,57−59] which due to their somewhat symmetric geometry could not provide such discrimination.

We repeated the same strategy for *ha*-Sy in the presence of each of the three other nucleotides (*ha*-Sy + C, *ha*-Sy + G, and *ha*-Sy + T), shown in Figures S1–S3. The resulting $T(E)$ values are displayed in Figure 6. Once again, panels Figure 6d–f show that the value of $T(E)$ depends on the orientation of the nucleotides (C, G, and T). For more clarity, Figure 7 shows the $T(E)$ of the *ha*-Sy in the presence of the four nucleotides for each angle of orientation in a wider window around the Fermi level. These results confirm that in a dynamic process like this, where the DNA passes through the *ha*-Sy with different nucleotides and angles of orientation, this device can discriminate between all possible cases and determine the correct sequence of such nucleotides. Note, however, that the differences in the Fermi level may be small for some cases but become larger for slightly different Fermi level positions. This also shows that it is possible to adjust the response and therefore the discrimination by changing the value of E_F.

Figure 7a shows that compared to the bare *ha*-Sy, all nucleotides with an angle of 0° increase $T(E)$. However, for other angles, the trend is not so obvious. In particular, for 90 and 180° (Figure 7b,c), both the *ha*-Sy + C and *ha*-Sy + T lead to increases of $T(E)$, while *ha*-Sy + A and *ha*-Sy + G lead to decreases. For 270° (Figure 7d) *ha*-Sy + C, *ha*-Sy + G, and *ha*-Sy + T lead to increases of $T(E)$, while *ha*-Sy + A leads to decreases. We explain these findings in terms of the interaction between the phosphate group of the nucleotide, which is a rather electronegative group, and the nanotube wall. The phosphate distorts the nanotube electronic structure when it is close to the nanotube wall and leads to nontrivial changes in the transmission. This distortion is further confirmed by

https://doi.org/10.1021/acsomega.3c04945
ACS Omega 2024, 9, 3240−3249

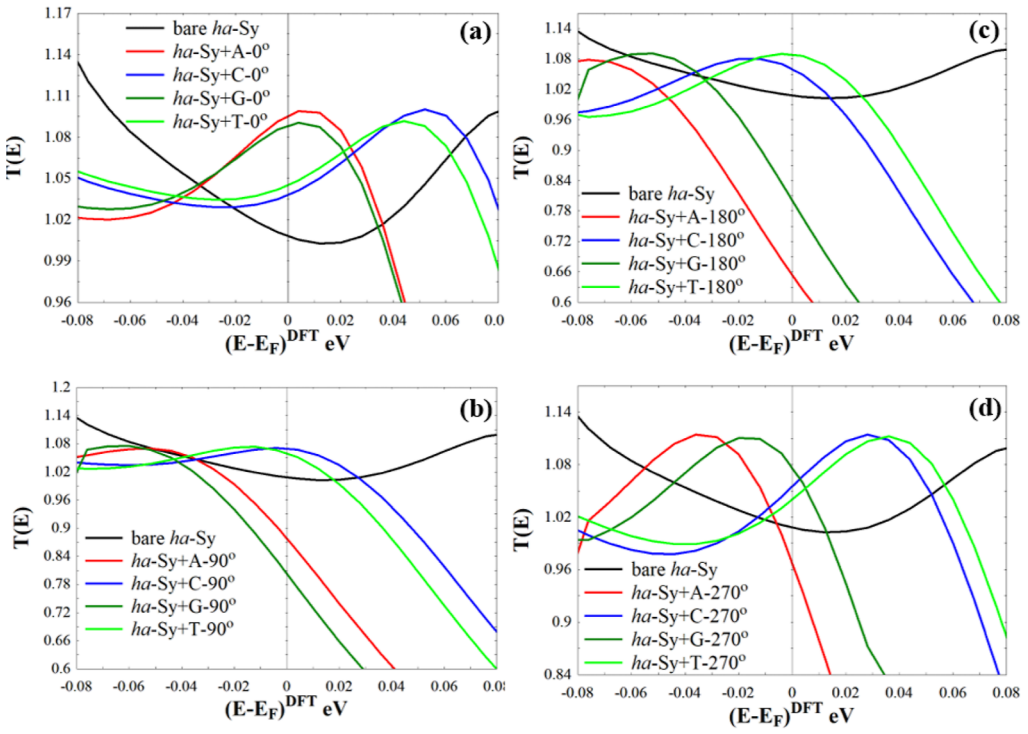

Figure 7. $T(E)$ of the *ha*-Sy + A, *ha*-Sy + C, *ha*-Sy + G, and *ha*-Sy + T, with the nucleotides rotate by (a) 0, (b) 90, (c) 180, and (d) 270° in a wider energy window (−0.08 to 0.08 eV) around E_F.

Table 2. Current of *ha*-Sy Calculated at 0.15 V with the Four Nucleotides (A, C, G, and T) and the Four Orientation Angles (0, 90, 180, and 270°)[a]

ha-Sy	current (A)	*ha*-Sy	current (A)	*ha*-Sy	current (A)	*ha*-Sy	current (A)
bare	0.314	bare	0.314	bare	0.314	bare	0.314
+A with 0°	0.249	+A with 90°	0.223	+A with 180°	0.205	+A with 270°	0.222
+C with 0°	**0.286**	+C with 90°	**0.256**	+C with 180°	0.236	+C with 270°	0.264
+G with 0°	0.255	+G with 90°	0.215	+G with 180°	0.211	+G with 270°	0.234
+T with 0°	0.282	+T with 90°	0.248	+T with 180°	**0.243**	+T with 270°	**0.270**

[a]The bold black numbers represent the highest current for each nucleotide.

studying the DOS and comparing it to the case of the isolated *ha*-Sy system, as can be seen in Figure S4, and the local DOS (LDOS) around the Fermi level, as can be seen in Figure S5. Since the distance between the phosphate and the wall depends on the associated nucleobase and the angle of rotation, the interaction of the whole nucleotide leads to nucleobase and angle selectivity. These results confirm that *ha*-Sy can selectively sense DNA nucleotides and therefore discriminate between different nucleobases and different orientations.

For more clarity and additional verifications, we calculated the current (I) for *ha*-Sy in the presence of the nucleotides, shown in Figures 3, S1−S3 at room temperature using the following equation[80]

$$I = \frac{Q_e}{h}\int \mathrm{d}E T(E)(f(E-\mu_L) - f(E-\mu_R)) \quad (1)$$

where $Q_e = |Q_e|$ is the electron charge, h is Planck's constant, $T(E)$ is the electronic transmission probability calculated using GOLLUM, f is Fermi−Dirac distribution function, $f(E-\mu) = \frac{1}{(1+e^{(E-\mu)/K_BT})}$, μ_L and μ_R are the electrochemical potentials of the left lead/right leads, respectively, and T is the temperature. The calculated currents for the four nucleotides and four orientation angles are shown in Figure 8, and the calculated values at 0.15 V are included in Table 2. Notice that for the *ha*-Sy with the nucleotides rotated by 0 and 90°, the *ha*-Sy + C shows the highest current, while with 180 and 270° such highest current corresponds to the *ha*-Sy + T. Note also that the measurement of very small values of current (nanoampere and picoampere) has been achieved and reported in previous works,[81−86] which implies that the obtained values of current and their differences shown in Table 2 can be used to selectively discriminate between nucleobases and angles, especially at relatively large voltages.

In addition, we also note that the fluctuations that appear around E_F in $T(E)$ should impact the Seebeck coefficient (S) amplitude of these systems. To demonstrate this, we compute S for the bare *ha*-Sy and the *ha*-Sy with the nucleotides, shown in Figure 9. From this figure, it is clear that there are differences between the obtained S values of the bare *ha*-Sy and the *ha*-Sy with the four nucleotides and angles. These differences can also be used for selective sensing of molecules using the Seebeck effect (Seebeck discriminated sensing). For more clarity, see Table S1, which shows the values of S shown in Figure 9. This provides again extra evidence of the capability of the *ha*-Sy as a DNA sequencer. Since both the conductance and the amplitude of S change upon rotation of the nucleotides

https://doi.org/10.1021/acsomega.3c04945
ACS Omega 2024, 9, 3240−3249

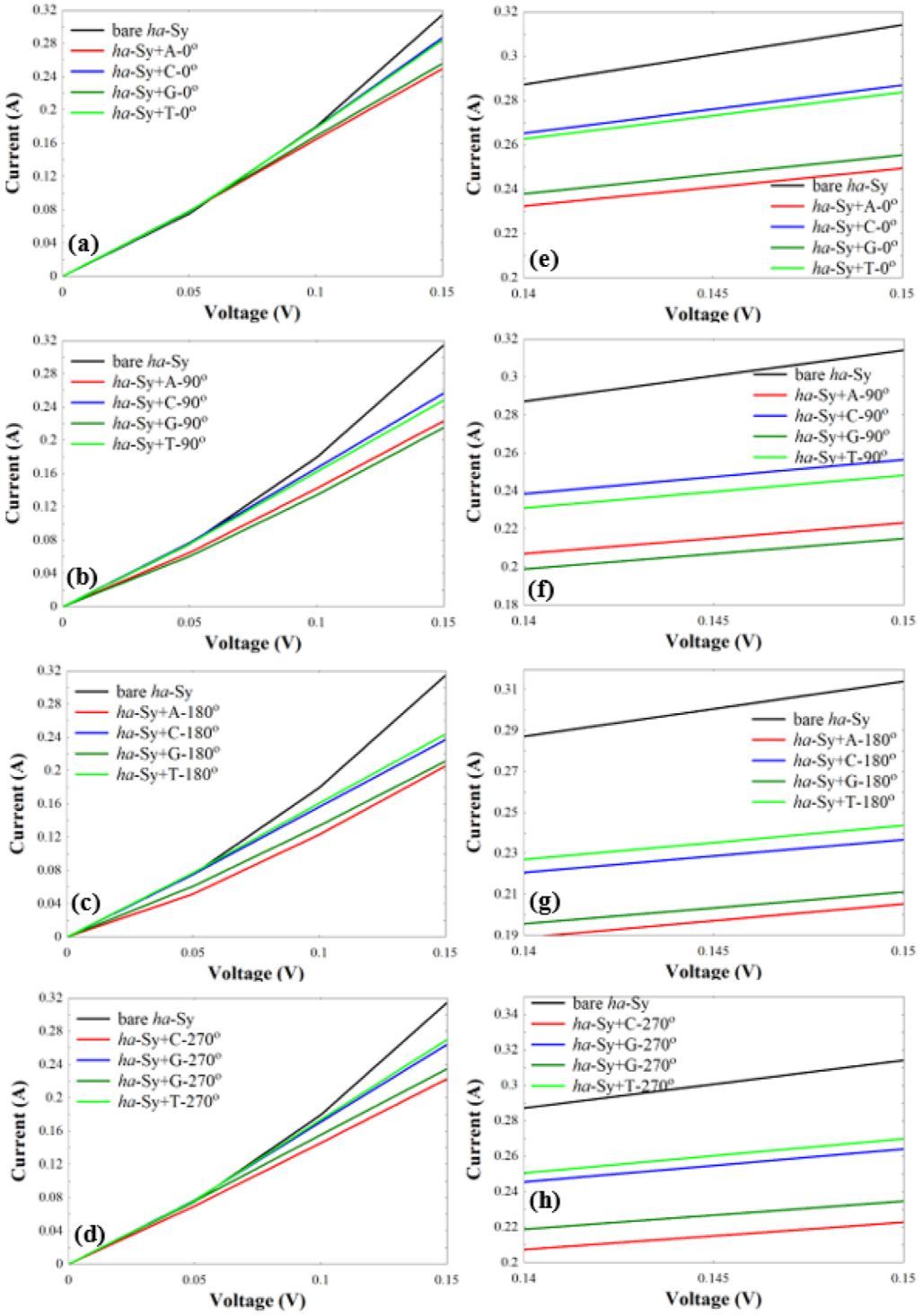

Figure 8. (a–d) Current of *ha*-Sy with the four nucleotides (A, C, G, and T) and the four orientation angles (0, 90, 180, and 270°) and (e–h) the same current shown within a narrow voltage window, ranging from 0.14 to 0.15 V.

inside the *ha*-Sy, these factors can be used together to minimize the error in the selective sensing process, leading thus to a robust tool for selective sensing of DNA nucleotides with similar electronic imprinting.

CONCLUSIONS

In summary, we have calculated from first principles the transport properties of the *ha*-Sy nanoscale sensor in the presence of the four nucleotides (A, C, G, and T) and with four angles of rotation (0, 90, 180, and 270°). The results show that this system, due to its asymmetric shape, is able to discriminate not only the type of nucleobase in the center of the nucleotide but also the angle of rotation. In particular, we have found that the transmission, conductance, current, and Seebeck coefficient have a substantial dependence on such factors. We explain these findings in terms of the interaction between the electronegative phosphate group and the nanotube wall, whose distance depends on the nucleobase

https://doi.org/10.1021/acsomega.3c04945
ACS Omega 2024, 9, 3240−3249

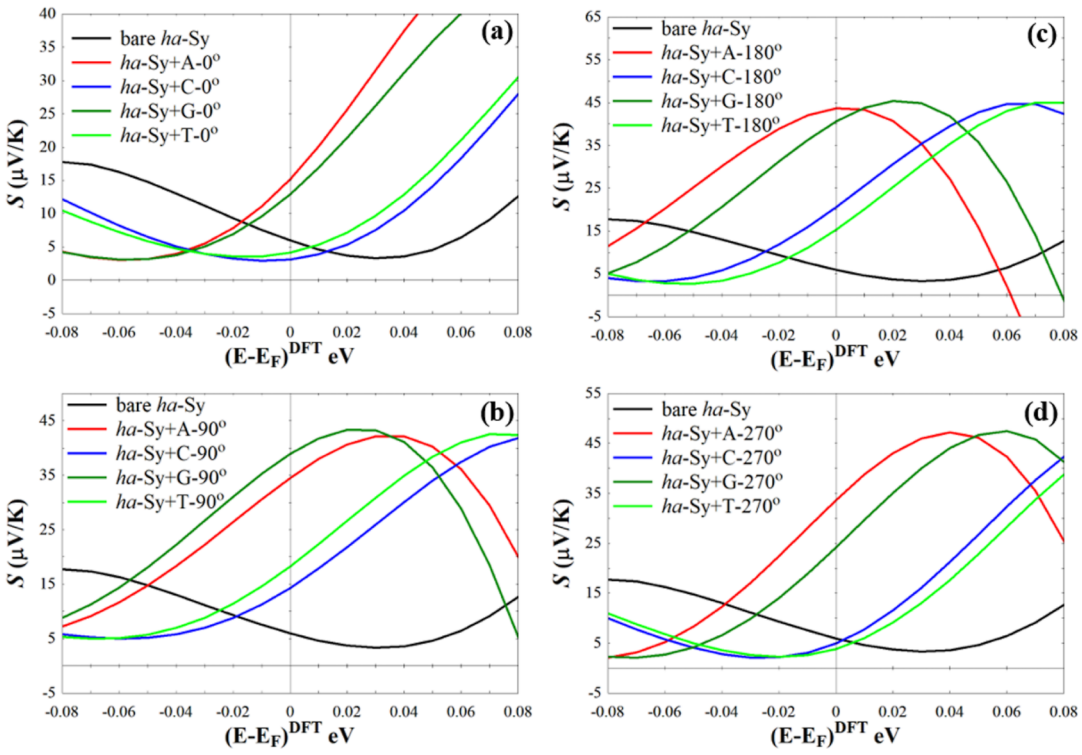

Figure 9. (a–d) Seebeck coefficient *S* of *ha*-Sy with the four nucleotides (A, C, G, and T) and four angles (0, 90, 180, and 270°).

and the angle of rotation. These results show that the carbon-nanotube-based sensor *ha*-Sy is able to effectively discriminate between different nucleobases and angles of rotation and open the door to the development of future fast and precise nanoscale sensors with tailored shapes.

■ ASSOCIATED CONTENT

Supporting Information

The Supporting Information is available free of charge at https://pubs.acs.org/doi/10.1021/acsomega.3c04945.

Additional figures, analysis and calculations: relaxed structures for the bases in the handle system not shown in Figure 4 (cytosine -C-, guanine -G-, and thymine -T-), DOS, LDOS, and Seebeck coefficient values (PDF)

■ AUTHOR INFORMATION

Corresponding Author

Víctor Manuel García-Suárez − *Departamento de Física, Universidad de Oviedo & CINN (CSIC), Oviedo 33007, Spain;* orcid.org/0000-0002-7392-4648; Email: vm.garcia@cinn.es, garciavictor@uniovi.es

Authors

Laith A. Algharagholy − *Department of Physics, College of Science, University of Sumer, Al-Rifai 64005 Thi-Qar, Iraq*

Sawsan S. Abaas − *Nasiriyah Directorate of Education, Ministry of Education, Nasiriyah 64001 Thi-Qar, Iraq*

Complete contact information is available at: https://pubs.acs.org/10.1021/acsomega.3c04945

Author Contributions

Laith A. Algharagholey, V. M. García-Suárez, and Sawsan S. Abaas were involved in interpreting the results and wrote and commented on the manuscript.

Notes

The authors declare no competing financial interest.

■ ACKNOWLEDGMENTS

L.A.A. acknowledges the Iraqi Ministry of Higher Education and Scientific Research and the University of Sumer for the support, and S.S.A. acknowledges the Iraqi Ministry of Education for the support. V.M.G.-S. acknowledges funding from the project PGC2018-094783 (MCIU/AEI/FEDER, EU).

■ REFERENCES

(1) Mardis, E. R. Next-generation DNA sequencing methods. *Annu. Rev. Genomics Hum. Genet.* **2008**, *9*, 387−402.

(2) Agah, S.; Zheng, M.; Pasquali, M.; Kolomeisky, A. B. DNA sequencing by nanopores: advances and challenges. *J. Phys. D: Appl. Phys.* **2016**, *49* (41), 413001.

(3) Shendure, J.; Aiden, E. L. The expanding scope of DNA sequencing. *Nat. Biotechnol.* **2012**, *30* (11), 1084−1094.

(4) Yang, H.; Liu, Y.; Gao, C.; Meng, L.; Liu, Y.; Tang, X.; Ye, H. Adsorption behavior of nucleobases on doped MoS2 monolayer: a DFT study. *J. Phys. Chem. C* **2019**, *123* (51), 30949−30957.

(5) Koowattanasuchat, S.; Ngernpimai, S.; Matulakul, P.; Thonghlueng, J.; Phanchai, W.; Chompoosor, A.; Panitanarak, U.; Wanna, Y.; Intharah, T.; Chootawiriyasakul, K.; et al. Rapid detection of cancer DNA in human blood using cysteamine-capped AuNPs and a machine learning-enabled smartphone. *RSC Adv.* **2023**, *13* (2), 1301−1311.

(6) Manna, A. K.; Pati, S. K. Theoretical understanding of single-stranded DNA assisted dispersion of graphene. *J. Mater. Chem. B* **2013**, *1* (1), 91−100.

(7) Cerf, A.; Alava, T.; Barton, R. A.; Craighead, H. G. Transfer-printing of single dna molecule arrays on graphene for high-resolution electron imaging and analysis. *Nano Lett.* **2011**, *11* (10), 4232−4238.

(8) Sadeghi, H.; Bailey, S.; Lambert, C. J. Silicene-based DNA nucleobase sensing. *Appl. Phys. Lett.* **2014**, *104* (10), 103104.

(9) Sadeghi, H.; Algaragholy, L.; Pope, T.; Bailey, S.; Visontai, D.; Manrique, D.; Ferrer, J.; Garcia-Suarez, V.; Sangtarash, S.; Lambert, C. J. Graphene sculpturene nanopores for DNA nucleobase sensing. *J. Phys. Chem. B* **2014**, *118* (24), 6908−6914.
(10) Dai, J.; et al. Target-triggered autonomous assembly of DNA polymer chains and its application in colorimetric nucleic acid detection. *J. Mater. Chem. B* **2016**, *4* (19), 3191−3194.
(11) Mantela, M.; Lambropoulos, K.; Simserides, C. Charge transport properties of ideal and natural DNA segments, as mutation detectors. *Phys. Chem. Chem. Phys.* **2023**, *25*, 7750−7762.
(12) Tsutsui, M.; Taniguchi, M.; Yokota, K.; Kawai, T. Identifying single nucleotides by tunnelling current. *Nat. Nanotechnol.* **2010**, *5* (4), 286−290.
(13) Ricci, F.; Gothelf, K. *Chemistry of DNA Nanotechnology Special Issue*; ACS Publications, 2023; pp 3−5.
(14) Liu, B.; Qi, Z.; Chao, J. Framework nucleic acids directed assembly of Au nanostructures for biomedical applications. *Interdiscip. Med.* **2023**, *1*, No. e20220009.
(15) Chen, X.; Yan, B.; Yao, G. Towards atom manufacturing with framework nucleic acids. *Nanotechnology* **2023**, *34*, 172002.
(16) Seeman, N. C.; Kallenbach, N. R. Design of immobile nucleic acid junctions. *Biophys. J.* **1983**, *44* (2), 201−209.
(17) Kearns, D. R. One-and Two-Dimensional NMR Studies of the Structures of Simple Sequence DNAs. *DNA—Ligand Interactions: From Drugs to Proteins*; Springer US, 1987, pp 23−43.
(18) Higuchi, R.; Dollinger, G.; Walsh, P. S.; Griffith, R. Simultaneous amplification and detection of specific DNA sequences. *Biotechnology* **1992**, *10* (4), 413−417.
(19) Yang, Z. A space-time process model for the evolution of DNA sequences. *Genetics* **1995**, *139* (2), 993−1005.
(20) Niemeyer, C. M. Self-assembled nanostructures based on DNA: towards the development of nanobiotechnology. *Curr. Opin. Chem. Biol.* **2000**, *4* (6), 609−618.
(21) Seeman, N. C. Nanomaterials based on DNA. *Annu. Rev. Biochem.* **2010**, *79*, 65−87.
(22) Erdem, A. Nanomaterial-based electrochemical DNA sensing strategies. *Talanta* **2007**, *74* (3), 318−325.
(23) Sun, H.; Ren, J.; Qu, X. Carbon nanomaterials and DNA: From molecular recognition to applications. *Acc. Chem. Res.* **2016**, *49* (3), 461−470.
(24) Chidchob, P.; Sleiman, H. F. Recent advances in DNA nanotechnology. *Curr. Opin. Chem. Biol.* **2018**, *46*, 63−70.
(25) Ying, Y.-L.; Hu, Z. L.; Zhang, S.; Qing, Y.; Fragasso, A.; Maglia, G.; Meller, A.; Bayley, H.; Dekker, C.; Long, Y. T. Nanopore-based technologies beyond DNA sequencing. *Nat. Nanotechnol.* **2022**, *17* (11), 1136−1146.
(26) Santana, J. E.; García, K. J.; De Santiago, F.; Miranda, Á.; Pérez-Figueroa, S. E.; González, J. E.; Pérez, L. A.; Cruz-Irisson, M. Selective sensing of DNA/RNA nucleobases by metal-functionalized silicon nanowires: A DFT approach. *Surf. Interfaces* **2023**, *36*, 102529.
(27) Djurišić, I.; Dražić, M. S.; Tomović, A. Ž.; Spasenović, M.; Šljivančanin, Ž.; Jovanović, V. P.; Zikic, R. DNA sequencing with single-stranded DNA rectification in a nanogap gated by N-terminated carbon nanotube electrodes. *ACS Appl. Nano Mater.* **2020**, *3* (3), 3034−3043.
(28) Min, S. K.; Kim, W. Y.; Cho, Y.; Kim, K. S. Fast DNA sequencing with a graphene-based nanochannel device. *Nat. Nanotechnol.* **2011**, *6* (3), 162−165.
(29) Prasongkit, J.; Feliciano, G. T.; Rocha, A. R.; He, Y.; Osotchan, T.; Ahuja, R.; Scheicher, R. H. Theoretical assessment of feasibility to sequence DNA through interlayer electronic tunneling transport at aligned nanopores in bilayer graphene. *Sci. Rep.* **2015**, *5* (1), 17560.
(30) Algharagholy, L. A.; Sadeghi, H.; Al-Backri, A. A. Selective sensing of 2, 4, 6-trinitrotoluene and triacetone triperoxide using carbon/boron nitride heteronanotubes. *Mater. Today Commun.* **2021**, *28*, 102739.
(31) Algharagholy, L. A.; Al-Galiby, Q. H.; Al-Backri, A. A.; Sadeghi, H.; Wabdan, A. A. Discriminating sensing of explosive molecules using graphene−boron nitride−graphene heteronanosheets. *RSC Adv.* **2022**, *12* (54), 35151−35157.
(32) Doshi, M.; Fahrenthold, E. P. Explosive molecule sensing at lattice defect sites in metallic carbon nanotubes. *Mater. Adv.* **2021**, *2* (19), 6315−6325.
(33) Farooqi, B. A.; Yar, M.; Ashraf, A.; Farooq, U.; Ayub, K. Graphene-polyaniline composite as superior electrochemical sensor for detection of cyano explosives. *Eur. Polym. J.* **2020**, *138*, 109981.
(34) Krepel, D.; Hod, O. Selectivity of a graphene nanoribbon-based trinitrotoluene detector: a computational assessment. *J. Phys. Chem. C* **2017**, *121* (39), 21546−21552.
(35) Roushani, M.; Shahdost-Fard, F.; Azadbakht, A. Using Au@nano-C60 nanocomposite as an enhanced sensing platform in modeling a TNT aptasensor. *Anal. Biochem.* **2017**, *534*, 78−85.
(36) Valentini, L.; Cantalini, C.; Armentano, I.; Kenny, J.; Lozzi, L.; Santucci, S. Highly sensitive and selective sensors based on carbon nanotubes thin films for molecular detection. *Diamond Relat. Mater.* **2004**, *13* (4−8), 1301−1305.
(37) Abbasi, M.; Nemati-Kande, E. Enhancing the reactivity of carbon-nanotube for carbon monoxide detection by mono-and co-doping of boron and nitrogen heteroatoms: A DFT and TD-DFT study. *J. Phys. Chem. Solids* **2021**, *158*, 110230.
(38) Rumyantsev, S.; Liu, G.; Potyrailo, R. A.; Balandin, A. A.; Shur, M. S. Selective sensing of individual gases using graphene devices. *IEEE Sens. J* **2013**, *13* (8), 2818−2822.
(39) Leve, Z. D.; Iwuoha, E. I.; Ross, N. The Synergistic Properties and Gas Sensing Performance of Functionalized Graphene-Based Sensors. *Materials* **2022**, *15* (4), 1326.
(40) Benjamin, S. R.; Miranda Ribeiro Júnior, E. J. GRAPHENE BASED ELECTROCHEMICAL SENSORS FOR DETECTION OF ENVIRONMENTAL POLLUTANTS. *Curr. Opin. Environ. Sci. Health* **2022**, *29*, 100381.
(41) Hwa, K.-Y.; Ganguly, A.; Santhan, A.; Sharma, T. S. K. Synthesis of water-soluble cadmium selenide/zinc sulfide quantum dots on functionalized multiwalled carbon nanotubes for efficient covalent synergism in determining environmental hazardous phenolic compounds. *ACS Sustainable Chem. Eng.* **2022**, *10* (3), 1298−1315.
(42) Xu, X.; Wang, X.; Chen, Y.; Liu, W.; Wang, S.; Yuan, F.; Ma, S. Design of MoS2/ZnO bridge-like hetero-nanostructures to boost triethylamine (TEA) sensing. *Vacuum* **2022**, *196*, 110733.
(43) Palaniappan, N.; Vashistha, N.; Aslam, R. Functionalized Carbon Nanotubes: Applications in Biosensing. *Functionalized Carbon Nanotubes for Biomedical Applications*; Wiley, 2023; p 97.
(44) Rahman, B. M. A.; Viphavakit, C.; Chitaree, R.; Ghosh, S.; Pathak, A. K.; Verma, S.; Sakda, N. Optical fiber, nanomaterial, and thz-metasurface-mediated nano-biosensors: A Review. *Biosensors* **2022**, *12* (1), 42.
(45) Kurbanoglu, S.; Cevher, S. C.; Toppare, L.; Cirpan, A.; Soylemez, S. Electrochemical biosensor based on three components random conjugated polymer with fullerene (C60). *Bioelectrochemistry* **2022**, *147*, 108219.
(46) Li, Z.; Zhang, W.; Xing, F. Graphene optical biosensors. *Int. J. Mol. Sci.* **2019**, *20* (10), 2461.
(47) Zhang, J.; Zhang, X.; Bi, S. Two-Dimensional Quantum Dot-Based Electrochemical Biosensors. *Biosensors* **2022**, *12* (4), 254.
(48) Zhong, X.; Mukhopadhyay, S.; Gowtham, S.; Pandey, R.; Karna, S. P. Applicability of carbon and boron nitride nanotubes as biosensors: Effect of biomolecular adsorption on the transport properties of carbon and boron nitride nanotubes. *Appl. Phys. Lett.* **2013**, *102* (13), 133705.
(49) Pettersson, E.; Lundeberg, J.; Ahmadian, A. Generations of sequencing technologies. *Genomics* **2009**, *93* (2), 105−111.
(50) Branton, D.; Deamer, D. W.; Marziali, A.; Bayley, H.; Benner, S. A.; Butler, T.; Di Ventra, M.; Garaj, S.; Hibbs, A.; Huang, X.; et al. The potential and challenges of nanopore sequencing. *Nat. Biotechnol.* **2008**, *26* (10), 1146−1153.
(51) Xu, M.; Fujita, D.; Hanagata, N. Perspectives and challenges of emerging single-molecule DNA sequencing technologies. *Small* **2009**, *5* (23), 2638−2649.

https://doi.org/10.1021/acsomega.3c04945
ACS Omega 2024, 9, 3240−3249

(52) Hu, P.; Zhang, J.; Li, L.; Wang, Z.; O'Neill, W.; Estrela, P. Carbon nanostructure-based field-effect transistors for label-free chemical/biological sensors. *Sensors* **2010**, *10* (5), 5133−5159.
(53) Dekker, C. Solid-state nanopores. *Nat. Nanotechnol.* **2007**, *2* (4), 209−215.
(54) Zwolak, M.; Di Ventra, M. Colloquium: Physical approaches to DNA sequencing and detection. *Rev. Mod. Phys.* **2008**, *80* (1), 141−165.
(55) Bayley, H. Sequencing single molecules of DNA. *Curr. Opin. Chem. Biol.* **2006**, *10* (6), 628−637.
(56) Ameur, A.; Kloosterman, W. P.; Hestand, M. S. Single-molecule sequencing: towards clinical applications. *Trends Biotechnol.* **2019**, *37* (1), 72−85.
(57) Kumawat, R. L.; Garg, P.; Bhattacharyya, G.; Pathak, B. Electronic transport through DNA nucleotides in BC3 nanogap for rapid DNA sequencing. *ACS Appl. Electron. Mater.* **2020**, *2* (5), 1218−1225.
(58) Wasfi, A.; Awwad, F.; Ayesh, A. I. Graphene-based nanopore approaches for DNA sequencing: A literature review. *Biosens. Bioelectron.* **2018**, *119*, 191−203.
(59) Wang, Y.; Zhao, Y.; Bollas, A.; Wang, Y.; Au, K. F. Nanopore sequencing technology, bioinformatics and applications. *Nat. Biotechnol.* **2021**, *39* (11), 1348−1365.
(60) Algharagholy, L.; Pope, T.; Al-Galiby, Q.; Sadeghi, H.; Bailey, S. W. D.; Lambert, C. J. Sensing single molecules with carbon−boron-nitride nanotubes. *J. Mater. Chem. C* **2015**, *3* (39), 10273−10276.
(61) Drummond, T. G.; Hill, M. G.; Barton, J. K. Electrochemical DNA sensors. *Nat. Biotechnol.* **2003**, *21* (10), 1192−1199.
(62) Giese, B. Electron transfer in DNA. *Curr. Opin. Chem. Biol.* **2002**, *6* (5), 612−618.
(63) Siriwong, K.; Voityuk, A. A. Electron transfer in DNA. *Wiley Interdiscip. Rev.: Comput. Mol. Sci.* **2012**, *2* (5), 780−794.
(64) Heller, D. A.; Jeng, E. S.; Yeung, T. K.; Martinez, B. M.; Moll, A. E.; Gastala, J. B.; Strano, M. S. Optical detection of DNA conformational polymorphism on single-walled carbon nanotubes. *Science* **2006**, *311* (5760), 508−511.
(65) Okada, T.; Kaneko, T.; Hatakeyama, R.; Tohji, K. Electrically triggered insertion of single-stranded DNA into single-walled carbon nanotubes. *Chem. Phys. Lett.* **2006**, *417* (4−6), 288−292.
(66) Qiu, X.; Ke, F.; Timsina, R.; Khripin, C. Y.; Zheng, M. Attractive Interactions between DNA−Carbon Nanotube Hybrids in Monovalent Salts. *J. Phys. Chem. C* **2016**, *120* (25), 13831−13835.
(67) Ramnani, P.; Saucedo, N. M.; Mulchandani, A. Carbon nanomaterial-based electrochemical biosensors for label-free sensing of environmental pollutants. *Chemosphere* **2016**, *143*, 85−98.
(68) Samuel, V. R.; Rao, K. J. A review on label free biosensors. *Biosens. Bioelectron.: X* **2022**, *11*, 100216.
(69) Guo, X.; Gorodetsky, A. A.; Hone, J.; Barton, J. K.; Nuckolls, C. Conductivity of a single DNA duplex bridging a carbon nanotube gap. *Nat. Nanotechnol.* **2008**, *3* (3), 163−167.
(70) Chen, X.; Guo, Z.; Yang, G. M.; Li, J.; Li, M. Q.; Liu, J. H.; Huang, X. J. Electrical nanogap devices for biosensing. *Mater. Today* **2010**, *13* (11), 28−41.
(71) Algharagholy, L.; Bailey, S. W. D.; Pope, T.; Lambert, C. J. Sculpting molecular structures from bilayer graphene and other materials. *Phys. Rev. B: Condens. Matter Mater. Phys.* **2012**, *86* (7), 075427.
(72) Tapasztó, L.; Dobrik, G.; Lambin, P.; Biró, L. P. Tailoring the atomic structure of graphene nanoribbons by scanning tunnelling microscope lithography. *Nat. Nanotechnol.* **2008**, *3* (7), 397−401.
(73) Algharagholy, L.; Pope, T.; Bailey, S. W. D.; Lambert, C. J. Electronic properties of sculpturenes. *New J. Phys.* **2014**, *16* (1), 013060.
(74) Liu, Z.; Suenaga, K.; Harris, P. J. F.; Iijima, S. Open and closed edges of graphene layers. *Phys. Rev. Lett.* **2009**, *102* (1), 015501.
(75) Zhang, J.; Xiao, J.; Meng, X.; Monroe, C.; Huang, Y.; Zuo, J. M. Free folding of suspended graphene sheets by random mechanical stimulation. *Phys. Rev. Lett.* **2010**, *104* (16), 166805.
(76) Huang, J. Y.; Ding, F.; Yakobson, B. I.; Lu, P.; Qi, L.; Li, J. In situ observation of graphene sublimation and multi-layer edge reconstructions. *Proc. Natl. Acad. Sci. U.S.A.* **2009**, *106* (25), 10103−10108.
(77) Soler, J. M.; Artacho, E.; Gale, J. D.; García, A.; Junquera, J.; Ordejón, P.; Sánchez-Portal, D. The SIESTA method for ab initio order-N materials simulation. *J. Phys.: Condens. Matter* **2002**, *14* (11), 2745−2779.
(78) Ceperley, D. M.; Alder, B. J. Ground state of the electron gas by a stochastic method. *Phys. Rev. Lett.* **1980**, *45* (7), 566−569.
(79) Ferrer, J.; Lambert, C. J.; García-Suárez, V. M.; Manrique, D. Z.; Visontai, D.; Oroszlany, L.; Rodríguez-Ferradás, R.; Grace, I.; Bailey, S. W. D.; Gillemot, K.; et al. GOLLUM: a next-generation simulation tool for electron, thermal and spin transport. *New J. Phys.* **2014**, *16* (9), 093029.
(80) Sadeghi, H. Theory of electron, phonon and spin transport in nanoscale quantum devices. *Nanotechnology* **2018**, *29* (37), 373001.
(81) Zhang, Y.; Duan, L. F.; Zhang, Y.; Wang, J.; Geng, H.; Zhang, Q. Advances in conceptual electronic nanodevices based on 0D and 1D nanomaterials. *Nano-Micro Lett.* **2014**, *6*, 1−19.
(82) Bylander, J.; Duty, T.; Delsing, P. Current measurement by real-time counting of single electrons. *Nature* **2005**, *434* (7031), 361−364.
(83) Ferrari, G.; Gozzini, F.; Molari, A.; Sampietro, M. Transimpedance amplifier for high sensitivity current measurements on nanodevices. *IEEE J. Solid-State Circuits* **2009**, *44* (5), 1609−1616.
(84) Sharma, D. K.; Ansari, M. A.; Saxena, A. K. A versatile automation program using LabVIEW for low dc current measurement. *J. Sci. Ind. Res.* **2014**, *73*, 91.
(85) Jing, W.; Binkang, L.; Linbo, R.; Geng, T.; Xianbao, L.; Hongguang, Q. Automatic weak-current measurement system with high precision. *High Power Laser Part. Beams* **2012**, *24* (8), 1975−1979.
(86) Krause, C.; Drung, D.; Scherer, H. Measurement of sub-picoampere direct currents with uncertainties below ten attoamperes. *Rev. Sci. Instrum.* **2017**, *88* (2), 024711.

https://doi.org/10.1021/acsomega.3c04945
ACS Omega 2024, 9, 3240−3249